nature biomedical engineering

ARTICLES

https://doi.org/10.1038/s41551-017-0157-y

Sustained miRNA delivery from an injectable hydrogel promotes cardiomyocyte proliferation and functional regeneration after ischaemic injury

Leo L. Wang[1], Ying Liu[2], Jennifer J. Chung[3], Tao Wang[2], Ann C. Gaffey[3], Minmin Lu[2], Christina A. Cavanaugh[2], Su Zhou[2], Rahul Kanade[3], Pavan Atluri[3], Edward E. Morrisey[2]* and Jason A. Burdick[1]*

MicroRNA-based therapies that target cardiomyocyte proliferation have great potential for the treatment of myocardial infarction. In previous work, we showed that the miR-302/367 cluster regulates cardiomyocyte proliferation in the prenatal and postnatal heart. Here, we describe the development and application of an injectable hyaluronic acid hydrogel for the local and sustained delivery of miR-302 mimics to the heart. We show that the miR-302 mimics released in vitro promoted cardiomyocyte proliferation over one week, and that a single injection of the hydrogel in the mouse heart led to local and sustained cardiomyocyte proliferation for two weeks. After myocardial infarction, gel–miR-302 injection caused local clonal proliferation and increased cardiomyocyte numbers in the border zone of a Confetti mouse model. Gel–miR-302 further decreased cardiac end-diastolic (39%) and end-systolic (50%) volumes, and improved ejection fraction (32%) and fractional shortening (64%) four weeks after myocardial infarction and injection, compared with controls. Our findings suggest that biomaterial-based miRNA delivery systems can lead to improved outcomes via cardiac regeneration after myocardial infarction.

Heart disease is the leading cause of mortality across the world—in the United States and Europe, heart disease contributes to 600,000 and 4,000,000 deaths each year, respectively[1,2]. Myocardial infarctions (MIs), or heart attacks, are individually linked to at least 50% of deaths[2]. During MI, blood supply to cardiac tissue is compromised, initiating a tissue remodelling response. Central to this process is the permanent loss of contractile cardiomyocytes, the native muscle cells in the heart, and the replacement of healthy tissue with non-contractile, fibrotic tissue. Improved management of acute MI through medical and surgical intervention has allowed up to 95% of patients to survive hospitalization[2]; however, many of these patients will develop chronic heart failure, resulting in a 50% mortality rate at five years post-MI[2].

Since a hallmark of MI is cardiomyocyte cell death, increasing the number of cardiomyocytes within the damaged myocardium may improve cardiac function. The major challenge to this approach is the limited capacity for renewal of cardiomyocytes in the adult heart[3,4]. Cardiomyocytes are often thought of as being terminally differentiated, exiting the cell cycle within the first week postnatally with low to non-existent levels of proliferation after injury[5,6]. This limited renewal capacity exacerbates the damage from ischaemic injury during MI, as damaged cells are replaced with fibrotic scar tissue rather than contractile cardiomyocytes[7].

Cellular therapy for cardiac regeneration remains an unmet challenge in the treatment of MI. Many cell types have been used in attempts to replace lost cardiomyocytes, including mesenchymal stem cells[8,9], skeletal myoblasts[10], and embryonic[11] or induced pluripotent stem cell-derived cardiomyocytes[12]. However, only cardiomyocytes derived from pluripotent stem cells have been shown to engraft and produce functional myocardium. An alternative to cell delivery is to promote endogenous cardiomyocyte proliferation using growth factors, small molecules and gene transfer[13–15]. Among these strategies, certain microRNAs (miRNAs) that induce cardiomyocyte proliferation have been identified, sometimes leading to improved cardiac function[16,17].

miRNAs are 18–22-nucleotide-long double-stranded RNAs that regulate gene expression post-transcriptionally by base-pairing with the 3′ untranslated region of target messenger RNAs and inhibiting their expression. In our previous work, we identified a cluster of miRNAs (miR-302/367) that induced proliferation in cardiomyocytes through a direct binding site on the 3′ untranslated region of large tumour supressor 2 (Lats2), Mps one binder (Mob1) and macrophage-stimulating 1 (Mst1), leading to the inhibition of Hippo signalling. Consequently, yes-associated protein (YAP), the transcriptional effector of the Hippo pathway, translocated to the nucleus to interact with the transcriptional enhancer factor domain (TEAD) family to activate gene expression pathways that promote cellular proliferation[18]. In mice, constitutive expression of the miR-302/367 cluster led to cardiomyopathy after MI due to persistent de-differentiation in cardiomyocytes. However, systemic daily administration of miR-302 mimics for one week after MI promoted cardiac regeneration by transiently reactivating the cardiomyocyte cell cycle to increase cell number, leading to proliferation and improved function. This work served as a proof of concept for miR-302 in regeneration; yet, systemic delivery had significant limitations, including potential off-target organ accumulation and the need for serial daily administrations.

Here, we demonstrate the use of local intramyocardial delivery of miR-302 mimics to infarcted myocardium via an injectable hydrogel, in an attempt to achieve miR-302 translation and overcome

[1]Department of Bioengineering, University of Pennsylvania, Philadelphia, PA, USA. [2]Department of Medicine, University of Pennsylvania, Philadelphia, PA, USA. [3]Division of Cardiovascular Surgery, Department of Surgery, University of Pennsylvania, Philadelphia, PA, USA. Leo L. Wang and Ying Liu contributed equally to this work. *e-mail: emorrise@mail.med.upenn.edu; burdick2@seas.upenn.edu

the limitations of systemic delivery. Hydrogels are water-swollen, cross-linked polymers capable of encapsulating and releasing therapeutics after injection into tissues[19,20]. Hydrogels have been explored widely for injection into cardiac tissue[21–26] and several formulations are currently in clinical trials and have been demonstrated as safe in large animals[27]. Hydrogels can be designed to undergo shear thinning, in which physical crosslinks are reversible under shear stress, allowing them to be injected through a syringe or catheter[28]. We previously developed shear-thinning, injectable hydrogels based on the guest–host interaction of modified hyaluronic acid (HA), a naturally occurring glycosaminoglycan[23–25]. HA was modified with β-cyclodextrin (CD, host) or adamantane (AD, guest), where CD and AD form complexes in a defined structural arrangement with high affinity ($K_a \cong 1 \times 10^5\ M^{-1}$). Thus, when CD-modified HA was mixed with AD-modified HA, they formed a hydrogel that exhibited shear-thinning behaviour during injection and rapid re-healing after removal of shear, permitting injection into cardiac tissue[22,23,25,29].

In this work, we show that this guest–host HA hydrogel system forms injectable gel–miR-302 complexes that release miR-302 to promote cardiomyocyte proliferation and regeneration after MI. Moreover, the gel–miR-302-induced cardiomyocyte proliferation led to the recovery of cardiac function. Thus, a combined gel–miRNA approach can be effectively used to promote mammalian cardiac regeneration through temporal specific activation of cardiomyocyte proliferation.

Results

Cholesterol-modified mimics and CD–HA interaction. We previously identified miR-302b and miR-302c as active miRNAs in the miR-302/367 cluster that modulate Hippo signalling, leading to cardiomyocyte proliferation[18]. To improve cellular uptake, miR-302b and miR-302c were modified with cholesterol on the 5′ end of the passenger strand. As previously reported, cholesterol-modified double-stranded RNAs are passively internalized by cells in vitro and in vivo, while unmodified RNAs are naturally repelled by cells due to electrostatics[30–33]. To ensure that cholesterol modifications improved miR-302 mimic uptake, miR-302b and miR-302c with and without cholesterol modifications were added to mouse neonatal cardiomyocytes in culture and cells were stained with antibodies against Ki67, a marker for proliferation. Cardiomyocytes treated with cholesterol-modified miR-302b and miR-302c mimics (miR-302–chol) were significantly more proliferative (Ki67$^+$) than those treated with unmodified mimics (Supplementary Fig. 1a,b). Moreover, treatment of cardiomyocytes with cholesterol-modified mimics also led to intracellular expression of miR-302 and knockdown of its Hippo signalling targets Lats2, Mob1 and Mst1 (Supplementary Fig. 1c,d)[18]. Subsequent studies were performed with equimolar amounts of miR-302b and miR-302c, hereafter termed miR-302.

Cholesterol is hydrophobic and has been well-described as a guest for interaction with CD as a host, suggesting that cholesterol-modified mimics may have improved affinity for CD–HA (Fig. 1a)[34,35]. To examine this interaction, we developed a fluorometric binding assay adapted from other similar assays[36,37]. Rhodamine B (Rho) fluorescence was quenched by CD–HA due to guest–host interactions between CD and Rho; however, cholesterol has a higher affinity for CD and should displace Rho and recover fluorescence. We observed that adding cholesterol-modified miR-302 increased the fluorescence of the solution, suggesting that cholesterol-modified miR-302 bound to CD–HA in a dose-dependent fashion (Fig. 1b and Supplementary Fig. 2a,b). In contrast, unmodified miR-302 did not change the solution fluorescence, suggesting minimal interaction (Supplementary Fig. 2c). Assuming negligible Rho binding, a binding constant for miR-302–chol–CD–HA complex formation was approximated as $K_a = 2.0 \times 10^3\ M^{-1}$ by fitting to the Benesi–Hildebrand equation, in agreement with previous reports (Supplementary Fig. 2d,e)[38]. Cholesterol-modified miR-302 mimics were then assembled into hydrogels with CD–HA and AD–HA (~20% modification of HA with either CD or AD, Supplementary Fig. 3). Release of cholesterol-modified miR-302 was sustained from hydrogels over three weeks (Fig. 1c), which was slower than the release of mimics without cholesterol, confirming the cholesterol–CD interaction (Supplementary Fig. 4).

To confirm that cholesterol-modified miR-302 did not affect the mechanical and erosion behaviour of hydrogels, we performed oscillatory rheology and hydrogel erosion assays with and

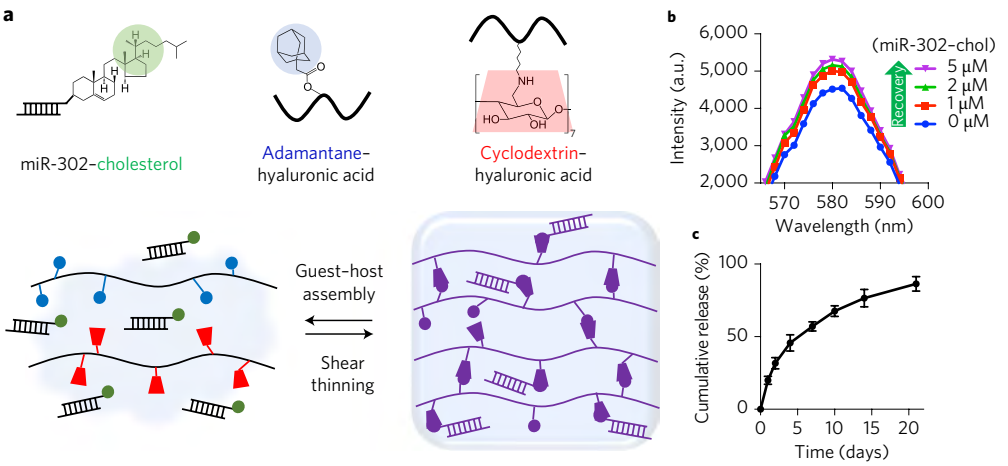

Fig. 1 | Hydrogel assembly and miR-302 interactions. a, HA modified with AD or CD self-assembled into shear-thinning and self-healing hydrogels. Likewise, cholesterol on miR-302 interacted with CD to sustain release from the hydrogel. **b**, Rhodamine/CD–HA interactions led to quenching of rhodamine fluorescence, but the fluorescence was recovered by titration of cholesterol-modified miR-302 into the system leading to displacement of rhodamine complexes, indicating complexation between cholesterol and CD. **c**, Release of cholesterol-modified miR-302b and miR-302c (210 μM of each) from hydrogels (5 wt%) in 1.5 ml microcentrifuge tubes over three weeks quantified by RiboGreen, a commercially available RNA quantification kit. Data are mean ± s.d., $n = 3$.

without encapsulated miR-302. Storage (G') and loss (G'') moduli were similar for hydrogels with and without miR-302 (Supplementary Fig. 5a). Shear-yielding and recovery were also observed in response to alternating high and low strain, demonstrating the ability of these hydrogels to thin under shear strain and rapidly reassemble on cessation of strain, permitting injection and rapid recovery of the hydrogel (Supplementary Fig. 5b). Hydrogel erosion was minimally affected by inclusion of cholesterol-modified miR-302 in the system (Supplementary Fig. 6). Taken together, cholesterol-modification of miR-302 mimics served to both enhance cellular uptake and improve affinity for the hydrogel without compromising mechanics, shear-thinning or erosion. All subsequent studies were performed with cholesterol-modified miR-302.

In vitro bioactivity of gel–miR-302 complexes. To assess the effect of the gel–miR-302 complexes on cardiomyocyte proliferation in vitro, supernatants from the hydrogel complexes with miR-302 (gel–miR-302) were collected and replaced serially over two weeks (Fig. 2a). Neonatal mouse cardiomyocytes were treated with supernatants from gel–miR-302 or controls and stained with 4,6-diamidino-2-phenylindole (DAPI) and antibodies to detect Ki67 and cardiac troponin T (cTnT). Gel–miR-302 complexes significantly enhanced proliferation (~20–25% positive for Ki67$^+$cTnT$^+$) from releasates collected from D0–D1, D1–D4 and D4–D7 compared with hydrogels with a non-specific sequence (gel–miR-NC) and hydrogels alone (~10% positive for Ki67$^+$cTnT$^+$ in both groups) (Fig. 2b,c). At early time intervals (D0–D1, D1–D4 and D4–D7), between ~0.15–0.3 μg μl^{-1} (5–10 μM) of miR-302 were released (Supplementary Fig. 7), which were biologically active concentrations (Supplementary Fig. 1) that induced neonatal cardiomyocyte proliferation. At later time intervals (D7–D10, D10–D14, D14–D21), ~0.1 μg μl^{-1} miR-302 were released, leading to minimal proliferation compared with controls. Since our previous study showed that transient delivery of miR-302 for one week could enhance cardiac function in vivo, the hydrogel release profile in vitro suggested that gel–miR-302 may replicate serial dosing for one week from a single hydrogel treatment.

In vivo bioactivity of gel–miR-302 after cardiac injection. Neonatal cardiomyocytes retain some proliferative capacity and therefore may be more responsive to miR-302 stimulation; thus, we sought to test the bioactivity of gel–miR-302 complexes in adult cardiomyocytes, which have extremely limited capacity to proliferate both in vitro and in vivo. Hydrogels were injected from 27G × 1/2″ tuberculin syringes into water to demonstrate their capacity for injection with rapid reassembly and minimal cargo loss (Fig. 3a). Gel-miR-302 or controls were then injected in two regions (2 × 5 μl) inferior and lateral to the proximal left anterior descending artery (LAD) in non-infarcted hearts of adult male mice, corresponding to the border zone of subsequent infarct models (Fig. 3b). At D5, D14 or D28, hearts were stained for markers of cardiac proliferation, Ki67 and phosphorylated histone H3 (pH3), and a marker of cytokinesis, Aurora B kinase (Aurora B). Sites of injection were identified from troponin-T-negative areas and proliferation in troponin-T-positive cardiomyocytes was quantified around these sites of injection for all three markers.

Gel–miR-302 injections significantly increased the proportion of Ki67$^+$ cardiomyocytes (Fig. 3c). Cardiomyocyte proliferation was sustained at D5 and D14 in gel–miR-302 compared with gel–miR-NC, but was no longer present by D28 (Fig. 3e). Gel–miR-302 also induced non-myocyte proliferation at D14 and D28, although at lower levels than both groups at D5 (Supplementary Fig. 8a). pH3$^+$ and Aurora B$^+$ cardiomyocytes around the site of gel–miR-302 injection were also elevated compared with controls at D5 (Fig. 3d), demonstrating up to ~3% and ~2%, respectively, of cardiomyocytes staining positive for these markers of proliferation and cytokinesis (Fig. 3f,g).

Of note, gel–miR-302 led to significantly more cardiomyocyte proliferation than PBS–miR-302 (Supplementary Fig. 8b), suggesting sustained release and improved retention of miR-302 by the hydrogel in vivo. Injections with gel–miR-NC also led to very low levels (<1%) of cardiomyocytes staining for Ki67, pH3 and Aurora B, corroborating the very rare and limited capacity for adult cardiomyocyte self-renewal[39,40]. Proliferating cardiomyocytes and non-myocytes were found within <200 μm of gel–miR-302 injection (Supplementary Fig. 8c). To confirm that cardiomyocytes were

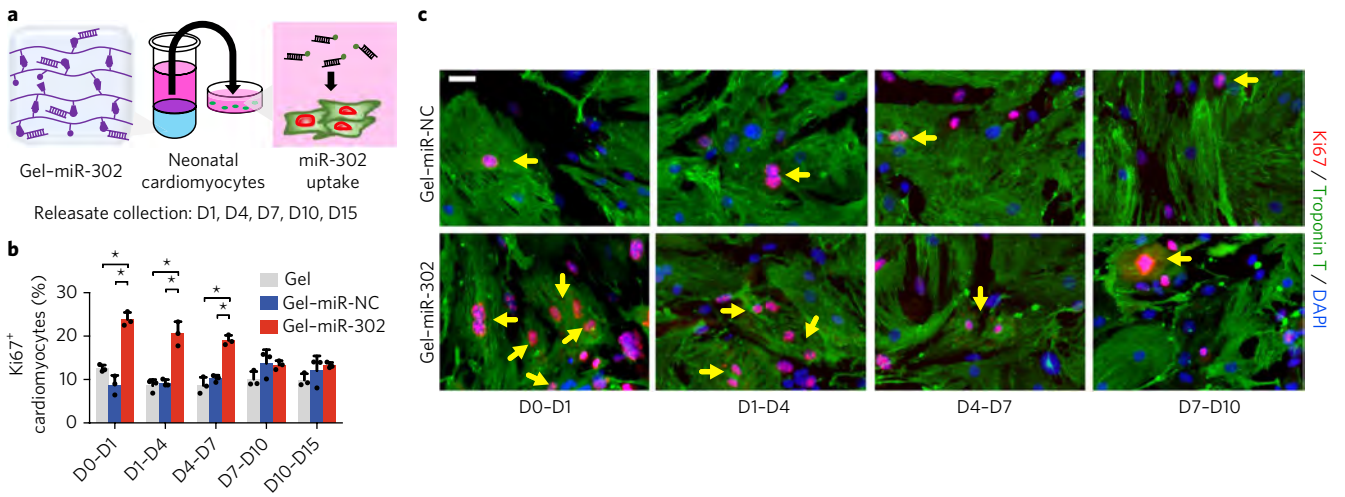

Fig. 2 | In vitro cardiomyocyte proliferation. a, Schematic of miR-302 supernatant collection and cardiomyocyte uptake. Gel–miR-302 (100 μl) complexes were formed in 1.5 ml microcentrifuge tubes with cholesterol-modified miR-302 (210 μM of miR-302b and miR-302c) or miR-NC (420 μM). Opti-MEM (500 μl) was added above hydrogels and supernatant was collected, frozen and replaced at D1, D4, D7, D10 and D15. Supernatants collected from each timepoint were added to primary neonatal cardiomyocytes in culture. At 48 h, cardiomyocytes were stained for Ki67, cTnT and with DAPI to detect proliferation. **b**, Quantification of Ki67$^+$cTnT$^+$ neonatal cardiomyocytes from hydrogel supernatants from D0–D1, D1–D4, D4–D7, D7–D10 and D10–D15 in vitro cultures demonstrating proliferative effects from early gel–miR-302 release up to seven days. Data are mean ± s.d., $n = 3$ per condition, $^*P < 0.05$. Quantification was based on counting of Ki67$^+$cTnT$^+$ co-stained cells relative to total cTnT$^+$ cells per high-power field. **c**, Representative images of Ki67$^+$cTnT$^+$ neonatal cardiomyocytes (yellow arrows) to demonstrate increased Ki67 staining up to seven days after exposure to gel–miR-302. Scale bar, 25 μm.

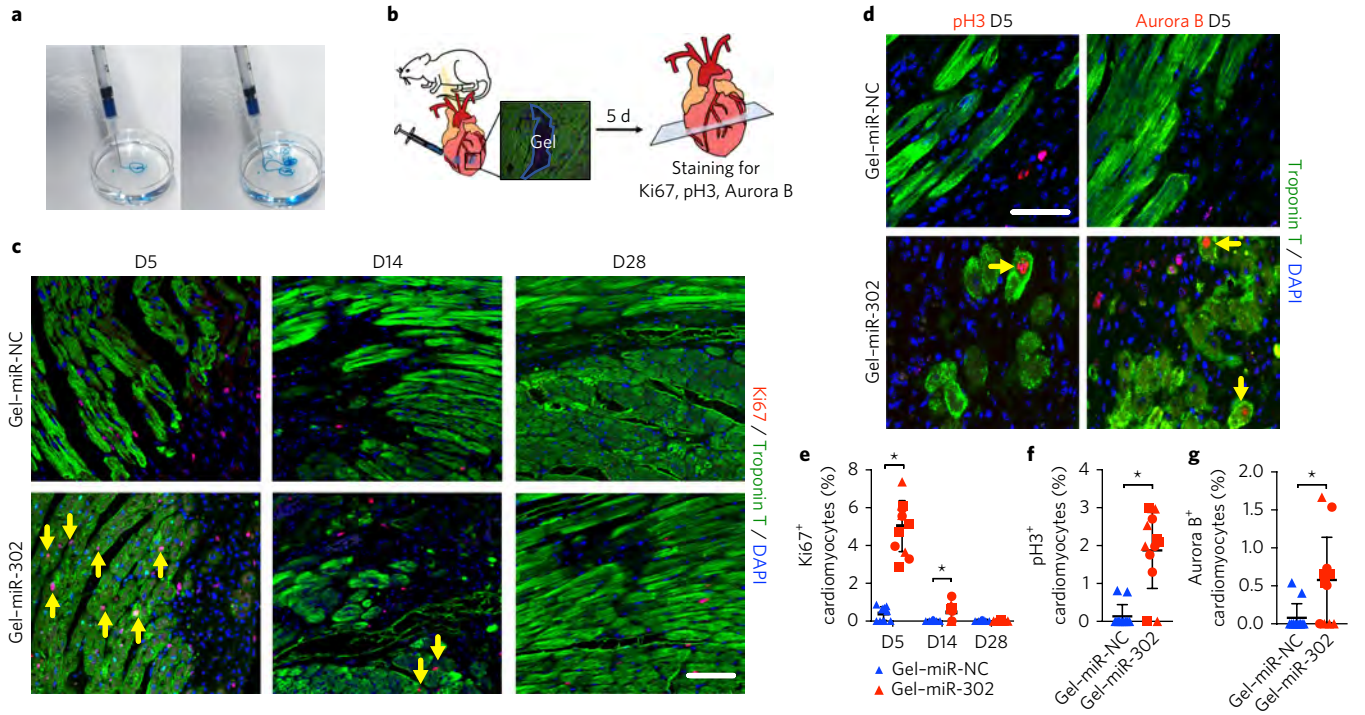

Fig. 3 | In vivo cardiomyocyte proliferation. a, Pre-formed hydrogel (5 wt%, blue dye) injected from a 27G × 1/2″ syringe into water, to demonstrate rapid reassembly and minimal dispersion of cargo on injection. **b**, Schematic for intramyocardial hydrogel injections into non-infarcted murine hearts. Two injections were made inferolateral to the proximal LAD below the left atrial appendage in non-infarcted mouse hearts after thoracotomy. At D5, D14 or D28, hearts were sectioned and stained for troponin T and Ki67, pH3 or Aurora B. **c**, Representative images of Ki67 staining in cardiomyocytes (yellow arrows) and non-myocytes at D5, D14 or D28, demonstrating increased proliferation in gel–miR-302-treated hearts. Scale bar, 50 μm. **d**, Representative images of pH3 and Aurora B staining in cardiomyocytes (yellow arrows) at D5. Scale bar, 50 μm. **e**, Quantification of cardiomyocytes ($Ki67^+cTnT^+$) from hearts treated with gel–miR-NC or gel–miR-302, demonstrating sustained proliferation of cardiomyocytes. **f**,**g**, Quantification of pH3- (**f**) and Aurora-B- (**g**) positive cardiomyocytes surrounding gel–miR-302 injection sites at D5, demonstrating increased proliferation in gel–miR-302-treated groups. For **e**–**g**, data are mean ± s.d., $n = 3$ animals per group, different symbol shapes indicate each animal, $^*P < 0.05$.

proliferating through inhibition of Hippo signalling, sections were stained for YAP. In gel–miR-302 sections, there was increased total YAP in the nucleus in support of our established mechanism by which YAP dephosphorylated and localized to the nucleus secondary to miR-302 (Supplementary Fig. 9)[18]. No differences in cardiomyocyte maturity were observed following stimulation (Supplementary Fig. 10).

Clonal proliferation in MHC–Confetti mouse model. To verify that the proliferation observed after gel–miR-302 treatment generated new cardiomyocytes after MI, lineage tracing analysis was performed using a multicolour R26R-Confetti Cre-reporter system with *loxP*-flanked nuclear green fluorescent protein (nGFP), red fluorescent protein (RFP), yellow fluorescent protein (YFP) and monomeric cyan fluorescent protein (mCFP) (Fig. 4a)[41]. The construct was designed such that random recombination activates only one of the four fluorescent protein genes, allowing stochastic labelling of target cells and their descendants with a single colour. This reporter system also allows cell-fate analysis using any inducible Cre activation mouse line (Fig. 4b)[41–43]. Confetti mice were bred with the Cre transgene expressed under the myosin heavy chain 6 (Myh6) promoter (Myh6-MerCreMer, also abbreviated MHC-MCM) to express Cre specifically in cardiomyocytes in response to tamoxifen[44]. In this system, Myh6-MerCreMer:R26R-Confetti-labelled cells and their daughter cells could express one of four different fluorescent reporters: nGFP, YFP, RFP or mCFP.

Tamoxifen doses were titrated to ensure low levels of $Myh6^+$ cardiomyocyte labelling so that individual clones could be identified (Supplementary Fig. 11a). At 14 days after tamoxifen administration, MI was induced by ligation of the LAD. Gel–miR-302 or gel–miR-NC (2 × 5 μl) was then injected adjacent to the infarct in the border zone. At 28 days after hydrogel injection, gel–miR-302-injected hearts were strongly labelled in the infarct border zones (Fig. 4c), suggesting increased lineage-labelled cardiomyocytes due to clonal expansion. In contrast, gel–miR-NC-injected hearts exhibited sparse labelling that mimicked hearts before injection (Supplementary Fig. 11b). Confocal imaging revealed expression of nGFP, RFP and YFP in adult hearts injected with both gel–miR-NC and gel–miR-302 (Supplementary Fig. 12a). In our hands, the expression of mCFP was too weak to reliably detect, as previously reported[41,42].

Clonal cardiomyocytes expressing nGFP, RFP and YFP were clearly identified in gel–miR-302-injected hearts while few clones were observed from gel–miR-NC injection (Supplementary Fig. 12a,b). Among labelled cardiomyocytes, multiple clusters expressing nGFP were detected in gel–miR-302-injected hearts and localized to the border zone of the infarction (Supplementary Fig. 12a). The average distance between $nGFP^+$ cells was significantly lower in gel–miR-302-treated groups, suggesting that these cells were derived from a common single cell (Supplementary Fig. 12c,d). Further analysis with wheat germ agglutinin (WGA) staining to identify cell membranes showed fluorescent cells within 50 μm were mostly contiguous in gel–miR-302-treated groups but not in gel–miR-NC groups (Fig. 5a). No differences in cardiomyocyte size were observed in the three fluorescent channels using WGA to distinguish between cardiomyocytes (Supplementary Fig. 12e). In gel–miR-NC groups, distant cells (>50 μm) were often interspersed by unlabelled cardiomyocytes.

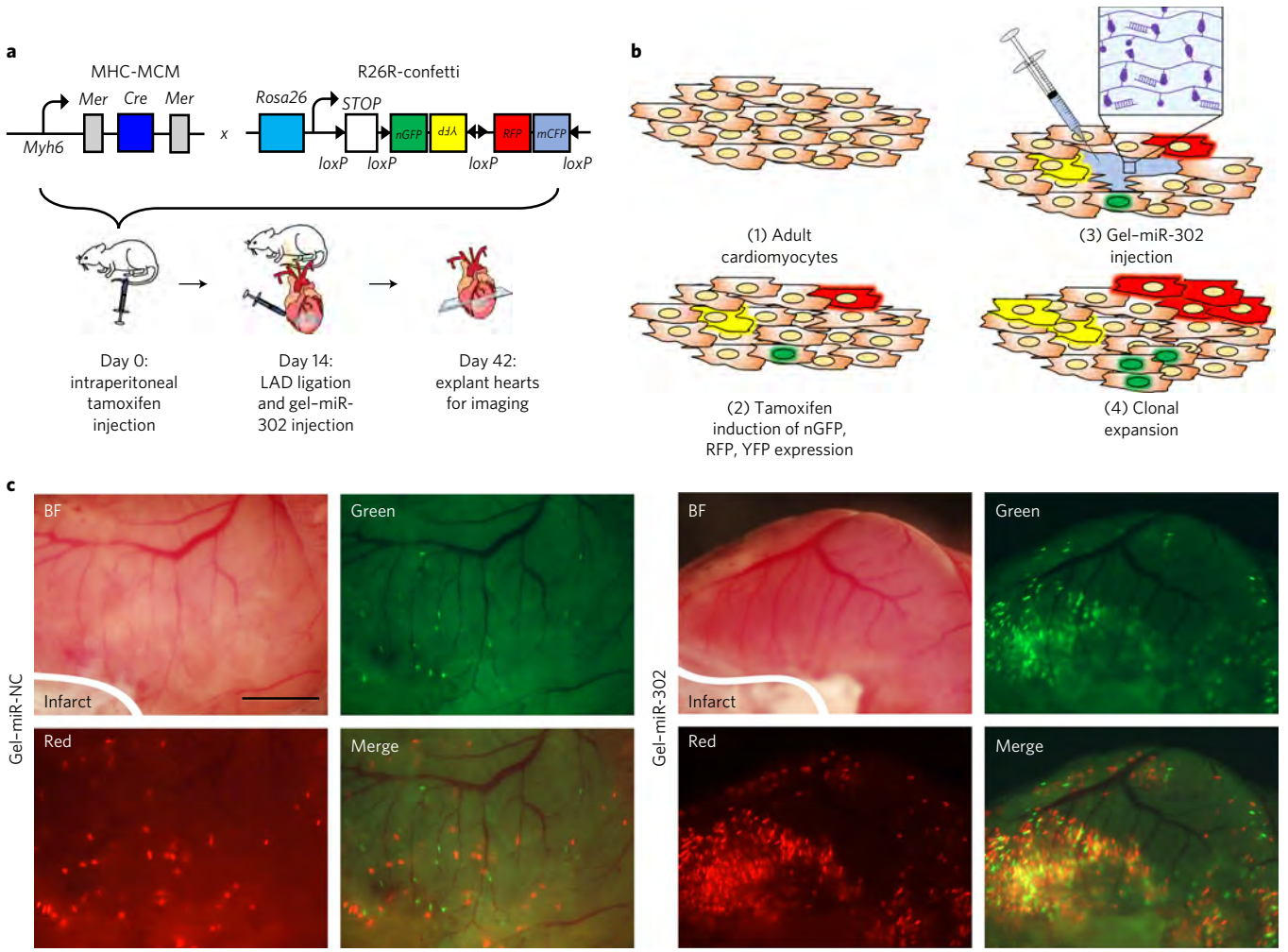

Fig. 4 | Gel–miR-302-induced clonal expansion in vivo. a, Schematic representation of lineage-tracing strategy and experimental design. To trace clonal proliferation, mice were cross-bred with Myh6-MerCreMer and R26R-Confetti. The expression of Myh6 leads to Cre–*loxP* recombination with consequent random activation of one of four fluorescent reporter proteins (nGFP, YFP, RFP and mCFP) with each colour representing a different clone from a Myh6 positive cardiomyocyte. In our experimental design, mice were injected with tamoxifen intraperitoneally to induce the stochastic expression of nGFP, RFP, YFP and mCFP. After 14 days, the LAD was ligated to induce ischaemic injury and gel–miR-302 or controls were injected in the border zone of the infarct downstream. At 28 days after ligation and injections, hearts were collected for analysis of clonal expansion. **b**, Mechanism for gel–miR-302-induced clonal expansion: (1) adult cardiomyocytes are non-proliferative and incapable of dividing after ischaemic injury; (2) tamoxifen is used to randomly label a small population of cardiomyocytes with one of four fluorescent reporter proteins; (3) hearts are infarcted and gel–miR-302 is injected into myocardium in the border zone; and (4) miR-302 stimulates differentiation, proliferation and expansion of fluorescently labelled cardiomyocytes, which pass the fluorescent protein gene onto daughter cells. **c**, Fluorescent scans of gross heart specimens immediately after explanting at 28 days. Fluorescence was displayed in the bright field (BF), green and red channels to indicate labelling of cardiomyocytes in both gel–miR-NC- and gel–miR-302-treated groups. Scale bar, 2 mm.

Using 50 μm as a standard, we quantified the number of cells to a single clone for nGFP, RFP and YFP across all sections of the heart in the border zone of infarcts. Gel–miR-302-injected hearts had a significant increase in the number of cells per clone (as many as eight), suggesting that these cells were derived from a common parent cell that had divided (Fig. 5b). Our results demonstrating expansion of clones paralleled those of other reports that have used this system[45–47].

Gel–miR-302 complex pharmacokinetics. To demonstrate that miR-302 mimics were localized and sustained in the heart after MI, the hydrogel was labelled with a near-infrared fluorescent molecule through a Michael addition between a thiolated Cy7.5 dye and methacrylated CD–HA (CD–Me–HA) (Supplementary Fig. 13)[23]. Cy7.5-labelled CD–HA was then assembled into hydrogels with miR-302 and injected into the heart following MI for ex vivo tracking at various times.

Immediately following injection, hydrogels exhibited intense signal surrounding the infarct at the two injection sites (Fig. 6a). This signal declined over the first week and distributed over the heart, where it dissipated by D28. Quantification demonstrated a reduction in radiant efficiency by ~90% over the first week, suggesting highest rates of clearance during this period (Fig. 6b). From qPCR, miR-302 expression in the heart was highest at D1, decreased over the first two weeks, and was similar to controls by D28 (Fig. 6c). The targets of miR-302, Lats2, Mob1 and Mst1, also decreased in the heart by D7, suggesting bioactivity of the gel–miR-302 complex in modulating these components of Hippo signalling (Fig. 6d). Low miR-302 expression was observed in the lungs at D7 (Supplementary Fig. 14), suggesting vascular drainage of miR-302 through the coronary sinus.

Cardiac function after MI and gel–miR-302 injection. Recognizing the ability of gel–miR-302 to induce both cardiomyocyte proliferation

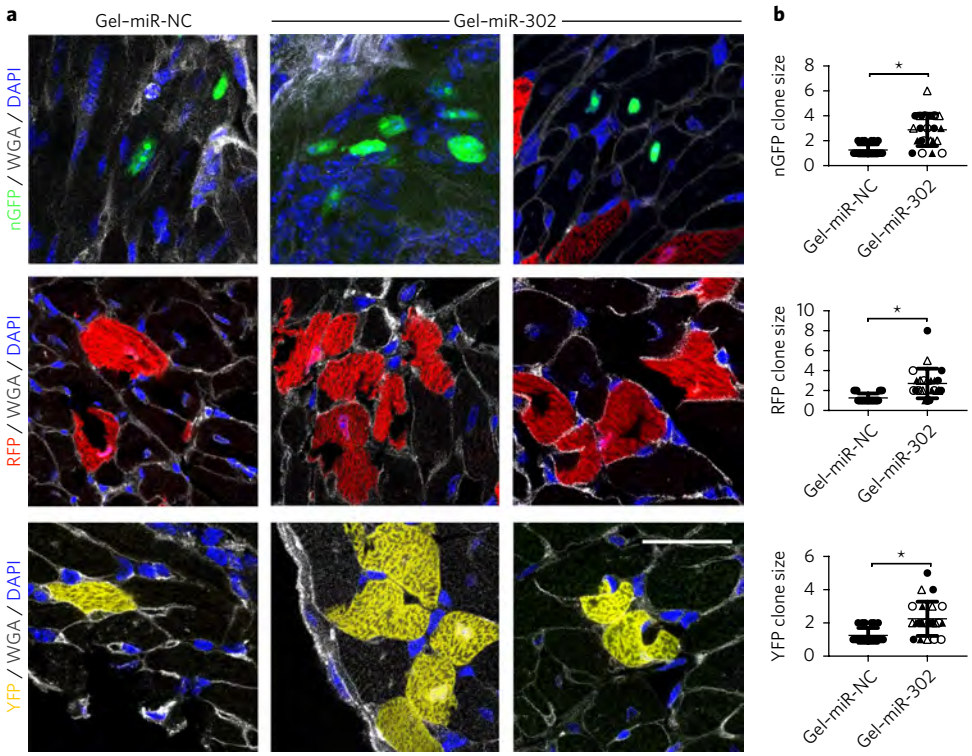

Fig. 5 | Clonal expansion of Confetti-labelled cardiomyocytes in mice. a, Representative sections from confocal imaging with labelled cardiomyocytes expressing nGFP, RFP or YFP. Gel–miR-NC sections consisted mostly of individual cardiomyocytes that were spatially separated. In gel–miR-302-treated groups, multiple clones were observed in all three fluorescent channels in close proximity, consisting of several daughter cells from a single parent cell. WGA (grey) separated individual cardiomyocytes and permitted identification of clones, specifically to differentiate multiple cardiomyocytes from multinucleated cardiomyocytes, whereas DAPI was used to stain cell nuclei. Scale bar, 50 μm. **b**, Quantification of clone size in the nGFP, RFP and YFP channels. Clones were identified as cells within 50 μm proximity to one another. Occurrences of one cell were also included in the quantification, although they are not technically clones. Data are mean ± s.d.; gel–miR-NC, $n = 3$; gel–miR-302, $n = 4$; different symbol shapes indicate each animal; $^*P < 0.05$.

and clonal proliferation, we examined the ability of gel–miR-302 injections to improve physiological outcomes after MI by echocardiography. Adult mice were selected to receive gel–miR-302, gel–miR-NC or PBS injection after MI. After four weeks, cardiac function was analysed through echocardiography and measurements of left ventricular end diastolic volume (LVEDV), left ventricular end systolic volume (LVESV), ejection fraction (EF) and fractional shortening (FS) were made. Gel–miR-302-treated mice had reduced cardiac remodelling, demonstrated by reductions in LVEDV and LVESV, measures of cardiac volumes at the beginning and end of a single contraction, respectively, compared with PBS or gel–miR-NC controls (Fig. 7a,b). LVEDV and LVESV of gel–miR-302-treated animals were not significantly different from non-infarcted mice. Whereas PBS and gel–miR-NC-treated animals had significantly reduced EF and FS, EF and FS of gel–miR-302-treated animals were not significantly different from non-infarcted mice (Fig. 7c,d). Masson's trichrome staining at four weeks showed that the smallest ventricular areas from axial sections were from gel–miR-302 treatment, while gross tissue specimens also demonstrated decreased infarct size (Fig. 7e). When quantified, gel–miR-302 appeared to decrease infarct size compared with gel–miR-NC from Masson's trichrome sections, although this effect was not statistically significant (Fig. 7f and Supplementary Fig. 15). Representative one-dimensional echocardiographic M-mode measurements of wall movement are shown (Fig. 7g), which illustrate improved anterior wall movement and decreased systolic and diastolic inner left ventricular diameters in gel–miR-302-treated mice. No changes in apoptosis or vascular density were observed at D28 between gel–miR-NC and gel–miR-302 treatments to suggest improvements were related to the cardiomyocyte response (Supplementary Figs. 16 and 17).

Discussion

The present study demonstrates that an engineered hydrogel, designed for injection and sustained delivery of miR-302, promotes both cardiomyocyte proliferation and functional regeneration. This approach overcomes the limitations of systemic delivery, which required seven days of serial intravenous injections for therapeutic benefit. The guest–host assembly mechanism was particularly attractive for this application as it permitted injection and self-healing to improve retention, and could potentially be adapted to minimally invasive delivery methods (for example, catheter). Lastly, the hydrogel was designed from HA, a component used in numerous clinical applications[48].

To further control-release, cyclodextrins involved in the guest–host assembly of the hydrogels sequestered cholesterol-modified miRNA. Interestingly, the binding of cholesterol to the cyclodextrin had minimal effects on hydrogel erosion and mechanics while sustaining the release of the miRNA mimics over three weeks in vitro, slower than when these interactions are not included. Because the mimics were released faster than hydrogel erosion, we believe that diffusion played a major role in the release, likely due to the dynamic interactions within the hydrogel and to the anionic repulsion between negatively charged HA and RNA. Mimic release may also be sustained due to the increase in size by cholesterol modification and by the ability of cholesterol to aggregate with itself due to hydrophobicity, causing entrapment within the network.

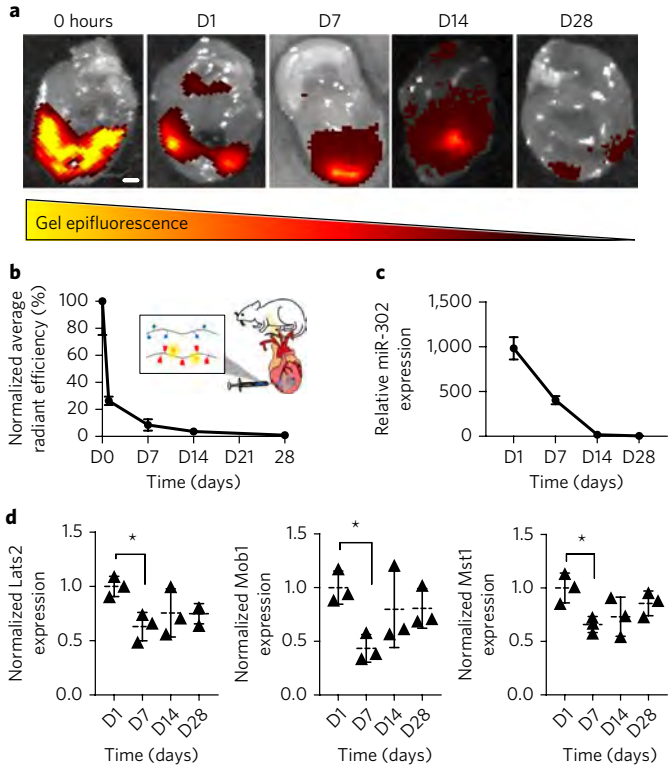

Fig. 6 | Hydrogel and miR-302 retention in mouse hearts. a, Images of hearts explanted and scanned following Cy7.5-gel–miR-302 complex injection in an MI model, demonstrating decreased hydrogel epifluorescence over time. Scale bar, 1 mm. **b**, Quantification of total radiant efficiency by normalizing to the initial signal intensity and to background autofluorescence, demonstrating rapid clearance over the first week. **c**, qPCR quantification of miR-302 in the heart at various times following gel–miR-302 injection, normalized to miR-302 expression from gel–miR-NC, indicating sustained miR-302 expression. **d**, qPCR expression of miR-302 targets Lats2, Mob1 and Mst1 in gel–miR-302-treated mice normalized to gel–miR-NC treated mice. For **b**–**d**, data are mean ± s.d., $n = 3$ mice per timepoint, $^*P < 0.05$.

In vitro, the gel–miR-302 complex led to proliferation in neonatal mouse cardiomyocytes in releasates collected as far out as seven days. The reduction in proliferation from releasates collected after this time (D10, D15) could be due to RNA degradation given the extended time of the experiment. Remarkably, in vivo, our gel–miR-302 complex led to robust proliferation of cardiomyocytes at D5 and D14 in the adult heart, a terminally differentiated organ. Expression of Aurora B kinase suggested that cardiomyocytes not only entered the cell cycle but were undergoing cytokinesis. Clonal expansion of cardiomyocytes was observed surrounding the infarct zone of the hearts treated with the gel–miR-302 complex. The use of a multicoloured lineage reporter allowed us to verify the generation of new cardiomyocytes rather than simply observing an increase in proliferative markers. Our findings concur with recent data showing that small numbers of newly generated cardiomyocytes observed over the lifespan of mammals or after injury are due to proliferation of pre-existing cardiomyocytes rather than arising from a progenitor population[39]. While these new cells may have enhanced contractility after MI, cardiomyocytes may have also played a role in limiting remodelling by signalling through paracrine factors to fibroblasts[49]. This explains the improvements in global cardiac volumes and function observed after delivery of the gel–miR-302 complex. Interestingly, while other hydrogels alone have improved function after MI, no improvement was observed in our case. This may be related to the softness (~500 Pa) and relative rapid clearance of our hydrogel in the heart. Previous hydrogel formulations that led to cardiac bulking were stiffer with higher retention[23,25].

The proliferative potential of the gel–miR-302 complex is further attributed to enhanced retention and sustained release of miR-302 mimics on injection, particularly as there was minimal proliferation without hydrogel. Complexing the miRNA with the hydrogel is likely to have protected the miRNA mimics from degradation by ubiquitous RNAse H-mediated mechanisms, allowing for continuous and persistent release of active mimics. This work also builds on previous reports of intramyocardial miRNA injections, where miRNAs were injected naked or in a lipid complex with a transfection reagent[50,51]. Since hydrogels allow for a single application and have been well-tolerated in human trials[27], we believe the use of a gel–miRNA complex offers significant advantages over these other approaches. Other recent reports have also corroborated the benefit of hydrogels in promoting miRNA delivery to the heart, although with different therapeutic targets or with viral delivery[52,53].

Our research demonstrates the potential of a bioengineered miRNA delivery approach to promote cardiomyocyte proliferation and cardiac regeneration after MI. This delivery mechanism has distinct advantages over current methods including: (1) overcoming the short lifespan of injected mimics, (2) use as a single application, (3) optimization of release of miRNA mimics over time for promoting cardiomyocyte proliferation and cardiac regeneration, and (4) potential for adaptation to percutaneous delivery through catheter. Currently, there are no approved treatments that regenerate myocardium; in this regard, our system may have unique improvements over other existing treatments for MI. Future studies to refine the gel–miRNA formulation in larger animal models of MI are important to progress the hydrogel formulation for in vivo delivery. Finally, this study establishes the proof of concept of a technology to permit minimally invasive, sustained miRNA delivery that can be tailored towards other small RNAs for application to cardiac and other tissues.

Methods

Material synthesis. Sodium hyaluronate 74 kDa (LifeCore) was converted to a tetrabutylammonium salt (HA–TBA) by exchange against Dowex-100 resin and neutralization by tetrabutylammonium hydroxide. CD–HA and AD–HA were synthesized as previously described[24]. Briefly, CD–HA was prepared by amidation between 6-(6-aminohexyl)amino-6-deoxy-β-cyclodextrin and HA–TBA in the presence of (benzotriazol-1-yloxy)tris(dimethylamino) phosphoniumhexafluorophosphate (BOP). AD–HA was synthesized by esterifi ation of HA–TBA with 1-adamantane acetic acid in di-*tert*-butyl bicarbonate (BOC_2O) and 4-dimethylaminopyridine (DMAP). Products were dialysed, frozen and lyophilized before use. ^{1}H NMR (Bruker) at 360 MHz was used to determine fi al product modifi ation, which was approximately 20% of HA disaccharide repeats for both CD–HA and AD–HA. Me–HA was synthesized by the esterifi ation reaction between HA and methacrylic anhydride and maintenance of pH between 7.5 and 8.5 for 8 h. Me–HA was then converted to a TBA salt (Me–HA–TBA) and subsequently modifi d with CD as previously mentioned. For Cy7.5 labelling, the fluorescent peptide GCKKG–Cy7.5 was synthesized by solid-phase peptide synthesis (Protein Technologies) using glycinol 2-chlorotrityl resin and 9-fluorenyl-methoxycarbonyl-protected amino acids that were then reacted with the free acid of Cy7.5. To couple the peptide to CD–Me–HA, the peptide was added dropwise to CD–Me–HA in PBS at pH 8 for 4 h.

Rheological characterization. Measurements were performed using an AR2000 stress-controlled rheometer (TA Instruments) fitted with a 20-mm-diameter cone and plate geometry, 59 min 42 s cone angle and 27 μm gap. Rheological properties were examined by time sweeps (1.0 Hz; 0.5% strain). For shear-recovery experiments, shear thinning was performed at 250% strain with recovery at 0.5% strain at 20 Hz.

miRNA purchase. All purchases were made as custom orders from GE Dharmacon. Their sequences are as follows.

Caenorhabditis elegans miR-67 (miR-NC):
5′-CGCUCAUUCUGCCGGUUGUUAUG-3′ (guide)
3′-AGAUGAGAAAGAUCCUCCAACACU-chol-5′ (passenger)
Mus musculus miR-302b (miR-302b):
5′-ACUUUAACAUGGGAAUGCUUUCU-3′ (guide)

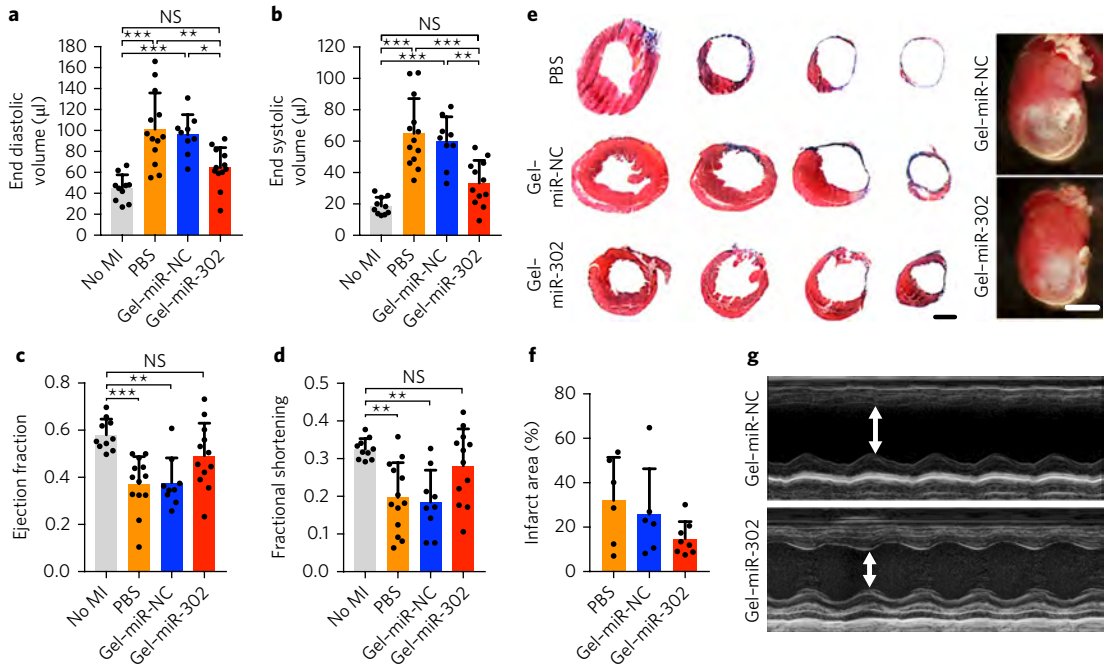

Fig. 7 | Functional outcomes after MI in adult mice. a,**b**, End diastolic (**a**) and end systolic (**b**) volumes at four weeks after MI in mice treated with PBS, gel–miR-NC or gel–miR-302 by B-mode echocardiography. Volume increases were significantly decreased in gel–miR-302-treated groups compared with controls. **c**,**d**, Ejection fraction (**c**) and fractional shortening (**d**) at four weeks after MI by echocardiography. Neither ejection fraction nor fractional shortening of gel–miR-302-treated mice were significantly different from non-infarcted mice. All groups were compared through one-way analysis of variance. Data are mean ± s.d.; no MI, $n = 10$; PBS, $n = 13$; gel–miR-NC, $n = 9$; gel–miR-302, $n = 12$; $^{*}P < 0.05$; $^{**}P < 0.01$; $^{***}P < 0.001$; NS, not significant. Outliers were removed using the robust regression and outlier removal method (ROUT) in Prism. **e**, Representative Masson's trichrome sections demonstrating cardiac volume improvement at D28. Sections are arranged from ligation to the apex (from left to right) to visualize changes in tissue remodelling. Scale bar, 2 mm. Representative gross heart pictures at D28 are also shown. Scale bar, 5 mm. **f**, Quantification of infarct size from Masson's trichrome. Infarct size was calculated from a minimum of three sections per animal where the scar was well-represented and expressed as infarct area (%) = (infarct area)/(total section area). Data are mean ± s.d. **g**, M-mode echocardiographs of left ventricular anterior and posterior walls demonstrating diminished motion in anterior wall of gel–miR-NC-treated mice with improvement in gel–miR-302-treated mice.

3′-GAUGAUUUUGUACCUUCGUGAAU-chol-5′ (passenger)
Mus musculus miR-302c (miR-302c):
5′-GCUUUAACAUGGGGUUACCUGC-3′ (guide)
3′-GGUGACUUUGUACCUUCGUGAA-chol-5′ (passenger)
Unmodified mimics did not have the cholesterol on the 5′ of the passenger strand.

Rhodamine quenching assay. Rhodamine B (50 ng μl^{-1}) was mixed with varying amounts of CD–HA (0–50 ng μl^{-1}) towards a final volume of 200 μl in deionized H_2O to determine saturating CD–HA concentrations for quenching. For unquenching assays, Rhodamine B (50 ng μl^{-1}) was quenched with 50 ng μl^{-1} CD–HA by mixing. Complexes were then mixed with miR-302 mimics (0–5 μM) in a final volume of 200 μl. Emission was measured on a Tecan Infinite200 96-well microplate reader at an excitation of 550 nm. miR-302b–chol affinity for Rho/CD–HA complexes was calculated by fit to the Benesi–Hildebrand equation.

miR-302 release and bioactivity. To form hydrogels with miRNA mimics, CD–HA (3.2 mg) or AD–HA (2.1 mg) polymers were sterilized under ultraviolet irradiation and resuspended in solutions of miR-302b (210 μM) and miR-302c (210 μM) in PBS under sterile conditions to a final polymer concentration of 5 wt%. Polymer–miRNA solutions of CD–HA and AD–HA were mixed manually and centrifuged. Hydrogels were incubated with Opti-MEM in 1.5 ml Eppendorf tubes with 500 μl supernatants collected and replaced at D1, D4, D7, D10, D15 and D21. Total miRNA concentration in releasates was quantified by RiboGreen (ThermoFisher) according to manufacturer's protocols. Briefly, 20 μl of releasate was incubated with Hi-Range RiboGreen Buffer in 1× Tris and ethylenediamine tetraacetic acid (EDTA) buffer to a final volume of 200 μl and fluorescence was measured at excitation of 500 nm and emission of 520 nm on a Tecan Infinite200 96-well microplate reader.

Neonatal cardiomyocyte isolation and culture. Ventricular cardiomyocytes from neonatal mice were isolated as described previously[17]. Briefly, ventricles from neonatal mice (postnatal day 0–3) were separated from atria, cut into pieces and then subjected to trypsin (0.5%) digestion buffer in calcium free Hank's Balanced Salt Solution (HBSS) containing 10 mM 4-(2-hydroxyethyl)-1-piperazineethanesulfonic acid (HEPES) and 0.54 mM EDTA under constant stirring. After digestion for 18 h at 4 °C, minced hearts were dissociated with calcium free HBSS supplemented with 10% horse serum, 5% fetal bovine serum (FBS) and 10 mM HEPES. Cells were then washed with calcium free Dulbecco's modified eagle media (DMEM) supplemented with 10% horse serum and 5% FBS. After a final wash, the cells were plated on uncoated plastic dishes for 2 h with media supplemented with 10% horse serum and 5% FBS. Non-attached cells were passed through a cell strainer (70 μm, BD Falcon) and seeded on a gelatin coated 96-well plate at a density of 15,000 cells per well. After incubation for 48 h, the majority of cells started to beat. Mouse ventricular cardiomyocytes prepared using this procedure consistently yielded a purity of >90%. For proliferation assays, gel–miR-302 releasates or controls were added to cells in 96-well plates for 24 h. After 48 h, cells were fixed with 4% paraformaldehyde for 15 min, permeabilized with 0.5% Triton X-100 in PBS solution for 10 min, followed by 30 min of blocking in 5% donkey serum (Jackson ImmunoResearch). Cells were then stained overnight at 4 °C with cardiac troponin T (ThermoFisher, MS295) and Ki67 (Abcam, ab16667) primary antibodies diluted in blocking solution and then secondary antibodies conjugated to Alexa Fluor488 and 555. Images were acquired with a Leica TCS SP8 microscope.

In vivo proliferation. Before use, polymers were sterilized under ultraviolet irradiation for 1 h. Hydrogels were formed with miRNAs as previously described and manually transferred to a 27G × 1/2″ U-100 tuberculin syringe (Terumo) under sterile conditions on ice. Male C57BL/6 mice (7–9 weeks) were selected to receive 10 μl total of gel-miR-302 or control injection (2 × 5 μl). Mice were anesthetized with 3% isoflurane in an induction chamber (2 l) and endotracheally intubated (Harvard Apparatus Regenerative Technology) with 1% isoflurane. A left lateral thoracotomy was performed at the fourth intercostal space to expose the heart. Injections were made inferolateral to the proximal LAD without infarct. Following injection, the chest was closed in three layers with a 3-0 polypropylene suture and animals were allowed to recover. After five days, the heart was excised, briefly washed in PBS, weighed, fixed in 4% paraformaldehyde, embedded in paraffin and further processed for immunofluorescence. Slides were washed in

PBS with 0.05% Triton X-100 (TBST) and blocked in 10% goat serum followed by incubation with primary antibodies against: cardiac troponin T (ThermoScientific, MS295), Ki67 (Abcam, ab16667), histone H3 phosphorylated at serine10 (Cell Signaling, 9701), Aurora B kinase (LSBio, LSB6592), YAP (Cell Signaling, 4912 S), von Willebrand factor (Abcam, ab8822), troponin I (Abcam, ab10231), ACTC1 (Abcam, ab46805). TUNEL staining (Invitrogen) was performed using the Click-iT Alexa Fluor596 kit according to manufacturer's protocols.
After 24 h, sections were incubated with secondary antibodies conjugated to Alexa Fluor488, 555 or 647 (Life Technologies). Nuclei were identified by counterstaining sections with DAPI (Vector Labs). Slides were then mounted in Vectashield (Vector Labs). A series of confocal images (z-stack) were acquired either by Leica STED Super-Resolution Microscope or LSM 710 Zeiss. Images were analysed and constructed by ImageJ software and Imaris (Bitplane). Cells were counted by two blinded independent investigators from a minimum of three representative sections per mouse. All animal procedures were performed in accordance with the Institutional Animal Care and Use Committee at the University of Pennsylvania.

MicroRNA extraction and expression of miR-302 and targets. Male C57BL/6 mice (7–9 weeks) were injected with either gel–miR-NC or gel–miR-302 (2×5 µl). At set time points after intramyocardial injection, the mice were euthanized and the heart, lung and liver were collected and rapidly snap frozen in liquid nitrogen for RNA extraction. RNA isolation was performed as previously described[54]. The Ambion mirVana miRNA Isolation Kit (ThermoFisher) was used to purify samples enriched with small RNA. Reverse transcription was performed using a TaqMan MicroRNA Reverse Transcription kit (Applied Biosystems) with 3 µl of RNA and RT primer sets (miR-302b: ID:000531) according to manufacturer's instructions. Quantitative real-time PCR was performed using the TaqMan MicroRNA assay kit (Applied Biosystems). Primers used for Lats2, Mob1 and Mst1 were ordered from Integrated DNA Technologies.
These primers were also used for qPCR amplification of these targets in neonatal cardiomyocytes.

Lats2 primers:
Forward: TAAGGGTCCTGCTTCCTGTGTTCT
Reverse: ACCTCTCATGTGAAAGAGGCCCAA
Mob1 primers:
Forward: CTGTGATCCAGCTTCAGGAGGAA
Reverse: TGCCAACTCTCGTCTGTCAA
Mst1 primers:
Forward: CAGGGCCTGCATAACATTTGCTGT
Reverse: TTCCTTGTCTGGCAAAGCCCAAAG

Confetti mouse generation. Mice were obtained by breeding Myh6-MerCreMer and R26R-Confetti reporter mice.

Primers to genotype Myh6-MerCreMer (MHC-MCM):
Forward: CGTTTTCTGAGCATACCTGGA
Reverse: ATTCTCCCACCGTCAGTACG
Primers to genotype R26R-Confetti:
Forward: AAAGTCGCTCTGAGTTGTTAT
Reverse: CCAGATGACTACCTATCCTC

Intraperitoneal tamoxifen (6.7 mg kg^{-1}) single injection was used to induce stochastic labelling of cardiomyocytes in Myh6-MerCreMer and R26R-Confetti mice. Doses were titrated to ensure low levels of cardiomyocyte labelling so that individual clones could be identified. Two weeks after tamoxifen injection, hearts were accessed by thoracotomy and the left ventricle was infarcted by ligation of the left anterior descending artery. Mice were selected to receive gel–miR-302 or gel–miR-NC (2×5 µl) injections lateral to the infarct in the border zone. Mice were euthanized 28 days post-surgery and gel-miR-302 injection to collect tissues. The hearts were fixed overnight with 2% paraformaldehyde. After 24 h, hearts were then transferred to 50% optimum cutting temperature compound (OCT), followed by continuous incubation in 100% OCT. Hearts in OCT were frozen with dry ice and kept at -80 °C until sectioning. For WGA staining, sections were rehydrated and then incubated for 1 h at room temperature with WGA conjugated to Alexa Fluor647 (Life Technologies, W32466) in PBS. Slides were then rinsed in PBS and mounted in Vectashield.

Myocardial infarction model. Male C57BL/6 mice (7–9 weeks) were selected to receive 10 µl total of gel–miR-302 or control injection (2×5 µl). Mice were anesthetized with 3% isoflurane in an induction chamber (2 l) and endotracheally intubated (Harvard Apparatus Regenerative Technology) with 1% isoflurane. A left lateral thoracotomy was performed at the fourth intercostal space to expose the heart. The LAD was ligated 2 mm below the left auricle and infarction was visualized from blanching of the left ventricle. Injections were made lateral to the infarct. The chest was closed in three layers with a 3–0 polypropylene suture and animals were monitored during recovery for signs of stroke or embolization. The number of mice for gel–miR-302 treatment group was at least 11 males to give 80% power to detect an effect size of 1.3 standard deviations using a two-group *t*-test with a 0.05 two-sided significance level. Injections were not blinded (due to variations in consistency between hydrogel and PBS) or randomized.

Near-infrared heart imaging. At D0, D1, D7, D14 and D28, mice were sacrificed and hearts were explanted and scanned on a LI-COR Pearl® Impulse Small Animal Imaging System (Lincoln, NE) with an excitation filter of 745 nm and emission filter for indocyanine green. Exposure time was set to 2 s and binning factor was set to 4. Intensity was expressed as radiant efficiency and the colour scale was set to a minimum of 1×10^7 and maximum of 1×10^8. Total radiant efficiency (photons s^{-1} cm^{-2} $steradian^{-1}$ per µW cm^{-2}) over hearts was normalized by manual measurements over the fluorescent region of interest, subtracting background measurements, and normalizing to initial radiant efficiency measurements as previously described[55].

Transthoracic echocardiography. Mice were anesthetized with 3% isoflurane induction following maintenance at 2% by nose cone. Hair was removed using Nair and limbs were taped onto the metal EKG leads. Echo was performed blinded using a VisualSonic Vevo 2100 system with a 40 MHz transducer for cardiac imaging. The transducer was placed parallel along the long axis of the left ventricle for a long axis view or rotated clockwise for short axis view. Images were analysed using Vevo200 1.6 VisualSonic software. Left ventricular internal diameters during systole (LVIDS) and diastole (LVIDD) were obtained from two-dimensional M-mode imaging, where fractional shortening was calculated per the equation EF = ((LVIDD −LVIDS)/LVIDD). LVESV and LVEDV were obtained from B-mode imaging by manually tracing the left ventricular endocardial border. Ejection fraction was calculated per the equation EF = ((LVEDV − LVESV)/LVEDV).

Statistical analysis. All statistical analyses were performed in Graphpad Prism 7. All data are reported as means ± s.d. and performed in triplicates unless otherwise indicated. For in vivo studies, there were a minimum of three mice per group unless otherwise indicated. Comparisons between two groups were performed by Students *t*-test with two-tailed criteria and significance determined at $P<0.05$. For comparison between multiple groups, significance was determined by one-way analysis of variance with post-hoc testing. Bonferroni correction was used to account for multiple comparisons, with $\alpha=0.05$. Normality was tested by D'Agostino and Pearson normality test and equal variances by Bartlett's test.

Life Sciences Reporting Summary. Further information on experimental design is available in the Life Sciences Reporting Summary.

Data availability. The authors declare that all data supporting the findings of this study are available within the paper and its supplementary information files.

Received: 13 March 2017; Accepted: 5 October 2017;
Published online: 27 November 2017

References

1. Townsend, N. et al. Cardiovascular disease in Europe: epidemiological update 2016. *Eur. Heart J.* **37**, 3232–3245 (2016).
2. Mozaff rian, D. et al. Heart disease and stroke statistics—2015 update: a report from the American Heart Association. *Circulation* **131**, e29–322 (2014).
3. Pasumarthi, K. B. S. Cardiomyocyte cell cycle regulation. *Circ. Res.* **90**, 1044–1054 (2002).
4. Jameel, M. N. & Zhang, J. Stem cell therapy for ischaemic heart disease. *Antioxid. Redox Signal.* **13**, 1879–1897 (2010).
5. Leone, M., Magadum, A. & Engel, F. B. Cardiomyocyte proliferation in cardiac development and regeneration: a guide to methodologies and interpretations. *Am. J. Physiol. Heart Circ. Physiol.* **309**, H1237–H1250 (2015).
6. Laflamme, M. A. & Murry, C. E. Heart regeneration. *Nature* **473**, 326–335 (2011).
7. Li, Y. et al. Acute myocardial infarction induced functional cardiomyocytes to re-enter the cell cycle. *Am. J. Transl. Res.* **5**, 327–335 (2013).
8. Orlic, D. et al. Bone marrow cells regenerate infarcted myocardium. *Nature* **410**, 701–705 (2001).
9. Elnakish, M. T. et al. Mesenchymal stem cells for cardiac regeneration: translation to bedside reality. *Stem Cells Int.* **2012**, 1–14 (2012).
10. Gavira, J. J. et al. Autologous skeletal myoblast transplantation in patients with nonacute myocardial infarction: 1-year follow-up. *J. Thorac. Cardiovasc. Surg.* **131**, 799–804 (2006).
11. Hodgson, D. M. et al. Stable benefit of embryonic stem cell therapy in myocardial infarction. *Am. J. Physiol. Heart Circ. Physiol.* **287**, H471–H479 (2004).
12. Lalit, P. A., Hei, D. J., Raval, A. N. & Kamp, T. J. Induced pluripotent stem cells for post-myocardial infarction repair: remarkable opportunities and challenges. *Circ. Res.* **114**, 1328–1345 (2014).
13. Korf-Klingebiel, M. et al. Myeloid-derived growth factor (C19orf10) mediates cardiac repair following myocardial infarction. *Nat. Med.* **21**, 140–149 (2015).
14. Ni, T. T. et al. Discovering small molecules that promote cardiomyocyte generation by modulating Wnt signaling. *Chem. Biol.* **18**, 1658–68 (2011).

15. Cheng, Y.-Y. et al. Reprogramming-derived gene cocktail increases cardiomyocyte proliferation for heart regeneration. *EMBO Mol. Med.* **9**, 251–264 (2017).
16. Liang, D. et al. miRNA-204 drives cardiomyocyte proliferation via targeting Jarid2. *Int. J. Cardiol.* **201**, 38–48 (2015).
17. Eulalio, A. et al. Functional screening identifies miRNAs inducing cardiac regeneration. *Nature* **492**, 376–381 (2012).
18. Tian, Y. et al. A microRNA-Hippo pathway that promotes cardiomyocyte proliferation and cardiac regeneration in mice. *Sci. Transl. Med.* **7**, 279ra38 (2015).
19. Panda, N. C. et al. Improved conduction and increased cell retention in healed MI using mesenchymal stem cells suspended in alginate hydrogel. *J. Interv. Card. Electrophysiol.* **41**, 117–127 (2014).
20. Teng, C. J., Luo, J., Chiu, R. C. J. & Shum-Tim, D. Massive mechanical loss of microspheres with direct intramyocardial injection in the beating heart: implications for cellular cardiomyoplasty. *J. Thorac. Cardiovasc. Surg.* **132**, 628–632 (2006).
21. Tous, E., Purcell, B., Ifkovits, J. L. & Burdick, J. A. Injectable acellular hydrogels for cardiac repair. *J. Cardiovasc. Transl. Res.* **4**, 528–542 (2011).
22. Gaffey, A. C. et al. Injectable shear-thinning hydrogels used to deliver endothelial progenitor cells, enhance cell engraftment, and improve ischaemic myocardium. *J. Thorac. Cardiovasc. Surg.* **150**, 1268–1277 (2015).
23. Rodell, C. B. et al. Shear-thinning supramolecular hydrogels with secondary autonomous covalent crosslinking to modulate viscoelastic properties in vivo. *Adv. Funct. Mater.* **25**, 636–644 (2014).
24. Rodell, C. B., Kaminski, A. L. & Burdick, J. A. Rational design of network properties in guest–host assembled and shear-thinning hyaluronic acid hydrogels. *Biomacromolecules* **14**, 4125–4134 (2013).
25. Rodell, C. B. et al. Injectable shear-thinning hydrogels for minimally invasive delivery to infarcted myocardium to limit left ventricular remodeling. *Circ. Cardiovasc. Interv.* **9**, e004058 (2016).
26. Wang, L. L. et al. Injectable, guest–host assembled polyethylenimine hydrogel for siRNA delivery. *Biomacromolecules* **18**, 77–86 (2016).
27. Seif-Naraghi, S. B. et al. Safety and efficacy of an injectable extracellular matrix hydrogel for treating myocardial infarction. *Sci. Transl. Med.* **5**, 173ra25 (2013).
28. Guvendiren, M., Lu, H. D. & Burdick, J. A. Shear-thinning hydrogels for biomedical applications. *Soft Matter* **8**, 260–272 (2012).
29. Mealy, J. E., Rodell, C. B. & Burdick, J. A. Sustained small molecule delivery from injectable hyaluronic acid hydrogels through host–guest mediated retention. *J. Mater. Chem. B* **3**, 8010–8019 (2015).
30. Liu, Y. M. et al. Cholesterol-conjugated let-7a mimics: antitumor efficacy on hepatocellular carcinoma in vitro and in a preclinical orthotopic xenograft model of systemic therapy. *BMC Cancer* **14**, 889 (2014).
31. Shim, M. S. & Kwon, Y. J. Effici t and targeted delivery of siRNA in vivo. *FEBS J.* **277**, 4814–27 (2010).
32. Wolfrum, C. et al. Mechanisms and optimization of in vivo delivery of lipophilic siRNAs. *Nat. Biotechnol.* **25**, 1149–1157 (2007).
33. Wang, L. L. & Burdick, J. A. Engineered hydrogels for local and sustained delivery of RNA-interference therapies. *Adv. Healthc. Mater.* **6**, 1601041 (2016).
34. van de Manakker, F., van der Pot, M., Vermonden, T., van Nostrum, C. F. & Hennink, W. E. Self-assembling hydrogels based on β-cyclodextrin/cholesterol inclusion complexes. *Macromolecules* **41**, 1766–1773 (2008).
35. López, C. A. et al. Molecular mechanism of cyclodextrin mediated cholesterol extraction. *PLoS Comput. Biol.* **7**, e1002020 (2011).
36. Politzer, I. R. et al. Effect of β-cyclodextrin on the fluorescence, absorption and lasing of rhodamine 6G, rhodamine B and fluorescein disodium salt in aqueous solutions. *Chem. Phys. Lett.* **159**, 258–262 (1989).
37. Mondal, A. & Jana, N. R. Fluorescent detection of cholesterol using β -cyclodextrin functionalized graphene. *Chem. Commun.* **48**, 7316 (2012).
38. López, C. A., de Vries, A. H. & Marrink, S. J. Molecular mechanism of cyclodextrin mediated cholesterol extraction. *PLoS Comput. Biol.* **7**, e1002020 (2011).
39. Senyo, S. E. et al. Mammalian heart renewal by pre-existing cardiomyocytes. *Nature* **493**, 433–436 (2012).
40. Ali, S. R. et al. Existing cardiomyocytes generate cardiomyocytes at a low rate after birth in mice. *Proc. Natl Acad. Sci. USA* **111**, 8850–8855 (2014).
41. Snippert, H. J. et al. Intestinal crypt homeostasis results from neutral competition between symmetrically dividing Lgr5 stem cells. *Cell* **143**, 134–144 (2010).
42. Lescroart, F. et al. Early lineage restriction in temporally distinct populations of Mesp1 progenitors during mammalian heart development. *Nat. Cell Biol.* **16**, 829–840 (2014).
43. Rios, A. C., Fu, N. Y., Lindeman, G. J. & Visvader, J. E. In situ identifi ation of bipotent stem cells in the mammary gland. *Nature* **506**, 322–327 (2014).
44. Sohal, D. S. et al. Temporally regulated and tissue-specific gene manipulations in the adult and embryonic heart using a tamoxifen-inducible Cre protein. *Circ. Res.* **89**, 20–25 (2001).
45. Frank, D. B. et al. Emergence of a wave of Wnt signaling that regulates lung alveologenesis by controlling epithelial self-renewal and differentiation. *Cell Rep.* **17**, 2312–2325 (2016).
46. Farin, H. F. et al. Visualization of a short-range Wnt gradient in the intestinal stem-cell niche. *Nature* **530**, 340–343 (2016).
47. Farin, H. F., Van Es, J. H. & Clevers, H. Redundant sources of Wnt regulate intestinal stem cells and promote formation of Paneth cells. *Gastroenterology* **143**, 1518–1529.e7 (2012).
48. Burdick, J. A. & Prestwich, G. D. Hyaluronic acid hydrogels for biomedical applications. *Adv. Mater.* **23**, H41–H56 (2011).
49. Tian, Y. & Morrisey, E. E. Importance of myocyte-nonmyocyte interactions in cardiac development and disease. *Circ. Res.* **110**, 1023–1034 (2012).
50. Yang, Y. et al. MicroRNA-34a plays a key role in cardiac repair and regeneration following myocardial infarction. *Circ. Res.* **117**, 450–459 (2015).
51. Lesizza, P. et al. Single-dose intracardiac injection of pro-regenerative microRNAs improves cardiac function after myocardial infarction. *Circ. Res.* **120**, 1298–1304 (2017).
52. Monaghan, M. G. et al. Exogenous miR-29B delivery through a hyaluronan-based injectable system yields functional maintenance of the infarcted myocardium. *Tissue Eng. Part A* https://doi.org/10.1089/ten.TEA.2016.0527 (2017).
53. Pandey, R. et al. MicroRNA-1825 induces proliferation of adult cardiomyocytes and promotes cardiac regeneration post ischaemic injury. *Am. J. Transl. Res.* **9**, 3120–3137 (2017).
54. Patel, R. S. et al. High resolution of microRNA signatures in human whole saliva. *Arch. Oral Biol.* **56**, 1506–1513 (2011).
55. Shcherbakova, D. M. & Verkhusha, V. V. Near-infrared fluorescent proteins for multicolor in vivo imaging. *Nat. Methods* **10**, 751–754 (2013).

Acknowledgements

The authors thank C. Loebel for assistance with manuscript revisions, C. Chen, C. Venkataraman, A. Trubelja, S. Zaman, J. Gordon and F. Arisi for assistance with mouse surgeries and histology, J. Galarraga and C. Rodell for material contribution and helpful discussion, S. Schultz of the Penn Small Animal Imaging Facility for assistance with echocardiography, and the Penn Histology and Gene Expression Core. This work was made possible by financial support from the American Heart Association through an established investigator award (J.A.B.) and predoctoral fellowship (L.L.W.), and the National Institutes of Health (F30 HL134255, UO1 HL100405, U01 HL134745).

Author contributions

L.L.W. and Y.L. contributed equally to this work. L.L.W., Y.L., E.E.M. and J.A.B. conceived the ideas and designed the experiments. L.L.W., Y.L., J.J.C., T.W., A.C.G., M.L., C.A.C., S.Z. and R.K. conducted the experiments and analysed the data. L.L.W., Y.L., P.A., E.E.M. and J.A.B. interpreted the data and wrote the manuscript. All authors have given approval to the final version of the manuscript.

Competing interests

Provisional patents concerning the technology described in this work have been filed.

Additional information

Supplementary information is available for this paper at https://doi.org/10.1038/s41551-017-0157-y.

Reprints and permissions information is available at www.nature.com/reprints.

Correspondence and requests for materials should be addressed to E.E.M. or J.A.B.

Publisher's note: Springer Nature remains neutral with regard to jurisdictional claims in published maps and institutional affiliations.

nature research

Corresponding author(s): Jason A. Burdick

☐ Initial submission ☐ Revised version ☒ Final submission

Life Sciences Reporting Summary

Nature Research wishes to improve the reproducibility of the work that we publish. This form is intended for publication with all accepted life science papers and provides structure for consistency and transparency in reporting. Every life science submission will use this form; some list items might not apply to an individual manuscript, but all fields must be completed for clarity.

For further information on the points included in this form, see Reporting Life Sciences Research. For further information on Nature Research policies, including our data availability policy, see Authors & Referees and the Editorial Policy Checklist.

Experimental design

1. Sample size

Describe how sample size was determined.

The number of mice for gel/miR-302 treatment group was at least 11 males to give 80% power to detect an effect size of 1.3 SDs using a two-group t test with a 0.05 two-sided significance level.

2. Data exclusions

Describe any data exclusions.

Outliers were removed using the robust regression and outlier removal method (ROUT) in Prism (1 animal in Gel/miR-NC group for Fig. 7a-d).

3. Replication

Describe whether the experimental findings were reliably reproduced.

In vitro studies were performed in triplicate or more (>3 gels per group) where noted. In vivo studies were performed in at least 3 animals per group where noted. Results were reliably reproduced between biological replicates.

4. Randomization

Describe how samples/organisms/participants were allocated into experimental groups.

This study was not randomized.

5. Blinding

Describe whether the investigators were blinded to group allocation during data collection and/or analysis.

For the histology studies, all IHC were quantified by two-blinded, independent observers (LLW, YL). For Confetti studies, images were quantified by a single-blinded observer (YL). For all in vivo injections, the surgeons (JJC, ACG, TW) were blinded to the treatment groups; however, it is clear immediately upon injection whether the treatment group contained gel or not, as there is added pressure required for product extrusion for the treatment groups with gel. Subsequently, the technician performing the echocardiography (S. Schultz, Penn Small Animal Imaging Facility) was blinded to all treatment groups. The analyzer of echocardiography (LLW) was blinded to the results for an initial subset of animals containing at minimum 5 animals per group but was subsequently not blinded, as additional animals were done in each group on separate days.

Note: all studies involving animals and/or human research participants must disclose whether blinding and randomization were used.

6. Statistical parameters

For all figures and tables that use statistical methods, confirm that the following items are present in relevant figure legends (or in the Methods section if additional space is needed).

n/a	Confirmed
☐	☒ The exact sample size (*n*) for each experimental group/condition, given as a discrete number and unit of measurement (animals, litters, cultures, etc.)
☐	☒ A description of how samples were collected, noting whether measurements were taken from distinct samples or whether the same sample was measured repeatedly
☐	☒ A statement indicating how many times each experiment was replicated
☐	☒ The statistical test(s) used and whether they are one- or two-sided (note: only common tests should be described solely by name; more complex techniques should be described in the Methods section)
☐	☒ A description of any assumptions or corrections, such as an adjustment for multiple comparisons
☐	☒ The test results (e.g. *P* values) given as exact values whenever possible and with confidence intervals noted
☐	☒ A clear description of statistics including central tendency (e.g. median, mean) and variation (e.g. standard deviation, interquartile range)
☐	☒ Clearly defined error bars

See the web collection on statistics for biologists for further resources and guidance.

Software

Policy information about availability of computer code

7. Software

Describe the software used to analyze the data in this study.	Image analysis was performed with ImageJ. Statistical analyssi was performed with Graphpad Prism 7.

For manuscripts utilizing custom algorithms or software that are central to the paper but not yet described in the published literature, software must be made available to editors and reviewers upon request. We strongly encourage code deposition in a community repository (e.g. GitHub). *Nature Methods* guidance for providing algorithms and software for publication provides further information on this topic.

Materials and reagents

Policy information about availability of materials

8. Materials availability

Indicate whether there are restrictions on availability of unique materials or if these materials are only available for distribution by a for-profit company.	All unique materials can be readily synthesized according to our protocols, and we can make them available. A detailed protocol was recently published (Loebel et al, Nature Protocols, 2017). We would be happy to assist others in this.

9. Antibodies

Describe the antibodies used and how they were validated for use in the system under study (i.e. assay and species).	The following antibodies were used: Cardiac Troponin T (ThermoScientific, MS295), Ki-67 (Abcam, ab16667), Histone H3 phosphorylated at serine10 (Cell Signaling, 9701), Aurora B kinase (LSBio, LSB6592), Yap (Cell Signaling, 4912S), von Willebrand Factor (Abcam, ab8822), Troponin I (Abcam, ab10231), ACTC1 (Abcam, ab46805). Each of these antibodies has been previously validated for IHC, and frequently used by the Penn Histology Core. They were used in accordance with the manufacturer's dilution recommendations.

10. Eukaryotic cell lines

a. State the source of each eukaryotic cell line used.	N/A
b. Describe the method of cell line authentication used.	N/A
c. Report whether the cell lines were tested for mycoplasma contamination.	N/A
d. If any of the cell lines used are listed in the database of commonly misidentified cell lines maintained by ICLAC, provide a scientific rationale for their use.	N/A

Animals and human research participants

Policy information about studies involving animals; when reporting animal research, follow the ARRIVE guidelines

11. Description of research animals

Provide details on animals and/or animal-derived materials used in the study.	Male C57BL/6 mice (7-9 weeks) were used in our studies. Confetti mice were obtained by breeding Myh6-MerCreMer and R26R-Confetti reporter mice.

Policy information about studies involving human research participants

12. Description of human research participants

Describe the covariate-relevant population characteristics of the human research participants.	N/A